PCCP

Accepted Manuscript

ROYAL SOCIETY OF CHEMISTRY

www.rsc.org/pccp

Physical Chemistry Chemical Physics
CREATED USING THE RSC LaTeX PCCP ARTICLE TEMPLATE – SEE www.rsc.org/electronicfiles FOR DETAILS
ARTICLE TYPE www. rsc.org/xxxxxx | XXXXXXXX

Shear dynamics of nanoconfined ionic liquids

Filippo Federici Canova,*[a] Hiroki Matsubara,[b] Masashi Mizukami,[c] Kazue Kurihara[a,c] and Alexander L. Shluger[a,d]

Received Xth XXXXXXXXXX 20XX, Accepted Xth XXXXXXXXX 20XX
First published on the web Xth XXXXXXXXXX 20XX
DOI: 10.1039/b000000x

We used molecular dynamics simulations to study the structure and shear dynamics of two ionic liquids (ILs) featuring the same cation 1-butyl-3-methyl-imidazolium or [BMIM], paired with bis(trifluoromethanesulphonyl)amide [NTF2] and tetrafluoroborate [BF4] anions, confined between two hydroxylated silica surfaces. The results demonstrate how the shape of IL molecules affects their layering structure at hydroxylated silica surfaces and how the layered structure of nanoconfined liquids determines their dynamical properties at molecular level. When [BMIM][NTF2] is sheared, larger molecular fluctuations in the inner layers are required to stabilise the system, and the resulting dynamics is irregular. The alternating charged layers in [BMIM][BF4] allow the system to stabilise through smaller oscillations, and the layers appear to shear on top of each other in a laminar fashion. The simulated dynamics explains qualitatively the relative change in viscosity that the two ILs exhibit when confined, as has been observed in previous experiments.

1 Introduction

Room temperature ionic liquids (ILs) refer to a class of salts with a relatively low freezing point[1], often consisting of a larger organic cation and an organic or inorganic anion[2]. These materials recently attracted a lot of scientific attention as the flexibility in the choice of the cation/anion molecules allows the properties of the liquid to be fine-tuned[3]. Besides the bulk liquid features, the behaviour of ILs at surfaces and in confined geometries is also of great interest for different fields, ranging from biological systems[4] to synthesis of nanomaterials, super-capacitors[5], micro/nano-fluidic[6], and lubrication[7]. It has been shown how ILs yield lower friction than conventional oils[8,9] and contribute to reducing wear in various systems[10–12] as they form a protective double layer with high local viscosity on the surfaces. These findings raised more interest within the tribology community towards characterising and designing new ionic liquid lubricants and additives[13] to target specific applications.

Recent investigations showed that frictional properties of bulk ILs can be different from those of confined fluids[14–16]. This is thought to result from the different molecular structure of the fluid induced by the interaction with a surface. While it is generally understood that molecules in bulk ILs should arrange in the pattern similar to binary ionic crystals, experiments[17] and simulations[18,19] shown how alternating layers of cations and anions can be formed at confining surfaces. This behaviour depends on surface properties[20] and the particular type of ions[21]. The relation between frictional properties and liquid ordering is so evident that it was exploited to directly control the friction coefficient by modifying the IL structure with external electric fields[22]. Despite the empirical evidence, the atomic scale information on the mechanisms of frictional processes and their relation to the fluid's structure is still not accessible to direct experiments. Therefore theoretical studies are vital for providing such information.

However, theoretical understanding of nanoscale friction and lubrication *per se* still poses a great challenge even in simple systems due to the complex nature of non-conservative interactions and their stochastic behaviour[23,24]. Molecular dynamics (MD) simulations are often limited to small systems and short time scales so that the sliding speed has to be orders of magnitude larger than in many experiments, making direct comparison with measurements particularly difficult. ILs are also not easy to model because many classical force fields are parametrised after *ab initio* calculations in the gas phase and reproduce structural properties of the fluid, but are not that accurate for the dynamical ones, overestimating the fluid viscosity[25]. The already slow diffusion of ILs in bulk liquid phase is expected to become even slower under confinement[26], which is the major issue since longer simulations are needed to reliably obtain average properties, such as the friction coefficient. For these reasons, even though many ILs have been exper-

[a] *Address, Advanced Institute for Materials Research, Tohoku University, 2-1-1 Katahira, Aoba-ku, Sendai 980-8577, Japan. E-mail: felix@wpi-aimr.tohoku.ac.jp*
[b] *Department of Applied Chemistry, School of Engineering, Tohoku University, Aobayama 6-6-07, Aoba-ku, Sendai 980-8579, Japan*
[c] *Institute of Multidisciplinary Research for Advanced Materials, Tohoku University, Katahira 2-1-1, Aoba-ku, Sendai 980-8577, Japan*
[d] *Department of Physics and Astronomy and the London Centre for Nanotechnology, University College London, Gower Street, London WC1E 6BT, United Kingdom*

imentally characterised, theoretical studies of their dynamic behaviour are still very few[27–30].

One of the first such theoretical study explored the lubrication mechanisms of ILs confined between alkylsilane monolayers adsorbed on SiO_2[27]. The incorporation of IL molecules between the organic chains caused the layer structure to become disordered, thus reducing the friction coefficient. Recent simulations showed how the friction coefficient of different ILs confined between two surfaces decreases on rough surfaces and this was attributed to the lower ordering of ions induced by the roughness[29]. Both studies point out the strong influence of ordering on friction; this behaviour is already understood for solid surfaces sliding against one another, but not for nanoconfined liquids. Under such conditions, the fluid is ordered by the interaction with the surfaces, but still not completely solidified. In this regime, the dynamical properties of the fluid are strongly dependent on the atomic details of the system, and their character still remains an open question. Answering this question may provide the guiding lines for designing and optimising ILs for lubrication and electrochemical applications where flow in nanoconfined spaces determines their performance.

To further our understanding of the nanoscale frictional mechanisms in ILs we performed MD simulations of the structure and shear dynamics of two ionic liquids featuring the same cation 1-butyl-3-methyl-imidazolium or [BMIM], paired with bis(trifluoromethanesulphonyl)amide [NTF2] and tetrafluoroborate [BF4] anions, confined between two hydroxylated silica surfaces. These ILs were previously investigated experimentally in Ref.[14] in carefully controlled conditions. Our results show how these two liquids arrange in clearly different structures above the same surface. In confined systems under shear stress, the different stability of the fluids structures causes the molecular flow of [BMIM][BF4] to be more regular than that of [BMIM][NTF2] and this explains the difference in the measurements.

2 Methods

2.1 Experimental Conditions

In this section we will briefly summarise the experimental details and main results from Ref.[14]. This is relevant because we designed the model systems in order to match those experimental conditions as much as possible, and this information should make the comparison with our results more clear.

The experimental system consists of pure [BMIM][NTF2] and [BMIM][BF4] confined between two silica surfaces in a modified surface force apparatus, allowing accurate detection of the separation distance between the plates. The amorphous silica surfaces are treated with water vapour prior to the measurements and are expected to be covered by silanol groups. The contact area between the two surfaces is measured with an interferometer and it is approximately 700 μm^2.

The top unit is driven into a lateral oscillation by a piezo-actuator and the resulting response is measured. Frictional properties of the confined fluids are measured from the amplitude response of the top unit as a function of driving frequency. The measurements were repeated at different separation distances, after gradually squeezing the fluids and the resonance curves were compared to the ones obtained in the absence of fluid, both at large separations and with the two surfaces in mechanical contact.

The bulk viscosity of [BMIM][NTF2] is smaller than [BMIM][BF4], as estimated from this as well as other experiments[31,32], but the situation becomes different in nanoconfined conditions. In particular, the data point out that the effective viscosity of [BMIM][NTF2] becomes larger than that of [BMIM][BF4]; the first liquid behaves more like a solid, while the latter remains fluid. The effect becomes most visible when the separation reaches roughly 2 nm. However, the origin of this behaviour is not understood and is one of the main topics of this study.

2.2 Atomistic Models

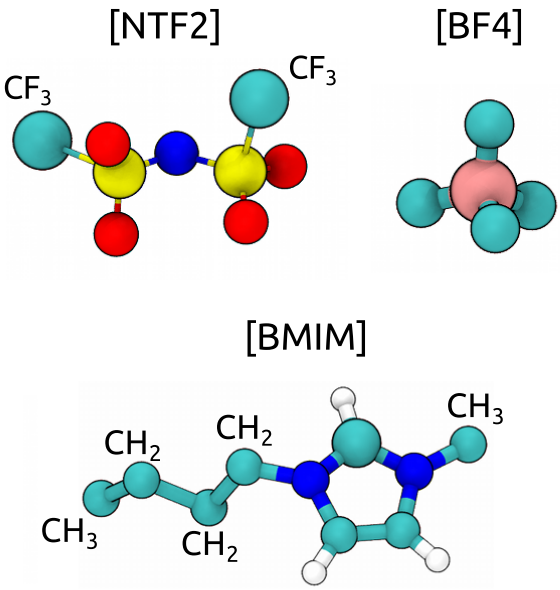

Fig. 1 (Colour online) Schematic representation of the united-atom models describing the IL molecules. The labels indicate the united atoms centres.

The ionic liquids were represented by a united-atom model from Ref.[33]. This particular model was chosen because it represents the bulk properties of the fluid as well as more complex all-atom models but with lower computational cost. All the

CH_3 and CH_2 groups of the cation, as well as the CF_3 groups of the [NTF2] anion are represented by single interaction centres, while H in the imidazolium ring is treated explicitly (see Fig. 1)

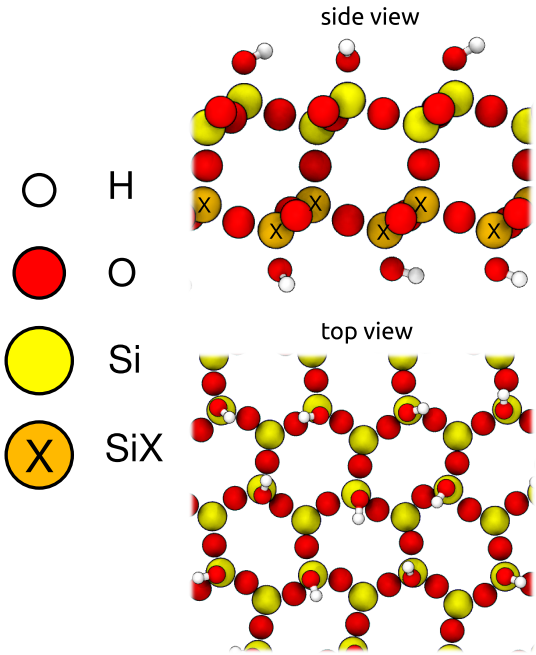

Fig. 2 (Colour online) Snapshots of the model silica surface from side and top view. SiX atoms have the same properties of Si but their atomic coordinates are not integrated during MD.

The silica slabs were built by cutting a $\beta-$cristobalite bulk crystal along the (111) direction, following a procedure similar to that described in Refs.[34,35]. Silicon atoms without full tetrahedral coordination were removed, leaving an oxygen terminated surface. One H atom is places above each under-coordinated O in the termination at an O-H distance of 0.1 nm. The O-H groups were then tilted around a random surface plane vectors in order to have a Si-O-H angle of 109.47° with random orientation. The same method of hydroxylation was applied to both surfaces of the slab in order to obtain a globally neutral slab and reduce effect of the surface dipole. This procedure yields a surface with 4.55 OH/nm^2 located at an average distance of 0.5 nm. A portion of the slab is shown in Fig. 2. The $\beta-$cristobalite model is often used in simulations because its density of 2.27 g/cm^3 is similar to that of amorphous silica, 2.2 g/cm^3 and force fields for the hydroxylated surface are available. Moreover, the density of silanol groups is comparable to the average experimental value of 4.9 OH/nm^2 measured for amorphous silica samples subject to maximum degree of hydroxylation[36], such as the ones used in the experiment described above.

The slabs used in our simulations consist of $10 \times 6 \times 1$ surface unit cells, with overall size of 5.035 nm and 5.232 nm along the x and y directions respectively, and thickness of 0.96 nm (Fig. 1). Periodic boundary conditions along the x and y directions are used in all calculations.

Interatomic interactions in the silica are modelled with the ClayFF force field[37]. All atoms in the slab are allowed to move, with the exception of one atomic layer of Si atoms, tagged SiX in Fig. 2, with fixed positions. The fixed layer is chosen to be the furthest from the IL-silica interface, and is used to externally control the lateral and vertical position of the slab.

Both IL and ClayFF force fields describe non-bonded interactions with Lennard-Jones potentials, thus all the mixed IL-silica interactions were treated in this way, and their parameters were determined with Lorentz-Berthelot mixing rules[38]. Electrostatic interactions were calculated with the PPPM solver[39]. The cutoff distance for short range and electrostatic (real space) interactions was set to 1 nm.

The temperature was regulated by coupling the whole simulated system to a Nose-Hoover thermostat[40,41], but, given the delicate nature of non-equilibrium simulations, we tested different coupling schemes. It was found that removing the thermostat caused the systems to heat up by 100 K in only a few nanoseconds, therefore having a thermostat was necessary. Average normal and lateral forces were not found to change considerably when the thermostat was applied exclusively to the surface atoms, nor when we switched to stochastic temperature control (Langevin's boundary conditions). All MD calculations were performed with the LAMMPS package[42].

The total force acting on the surfaces was calculated as:

$$\vec{F}^{slab}(t) = \sum_{i}^{slab} \left\langle \vec{f}_i(t+\tau) \right\rangle_{1\,\mathrm{ps}}, \qquad (1)$$

where $\vec{f}_i(t)$ is the force on the i-th atom at a given time t and the averaging is done over time intervals $\tau \in (0,1)$ ps. The summation extends over all atoms in either the *top* or *bottom* slab.

The normal load acting on the fluid was calculated as:

$$L(t) = F_z^{top}(t) - F_z^{bottom}(t) \qquad (2)$$

where $F_z^{top}(t)$ and $F_z^{bottom}(t)$ are the total normal forces for the upper and lower slab, respectively, at a given time t, as calculated from equation 1.

2.3 Designing the confined system

The computational systems to study the shear dynamics of our liquids in nanoconfined conditions can be obtained by placing a predetermined number of IL molecular pairs between two

model silica surfaces. We chose the separation distance between the surfaces to be $h \approx 2.0$ nm, where, according to the experiment, the different behaviour of the two liquids becomes most distinct. The number of molecules inside such volume

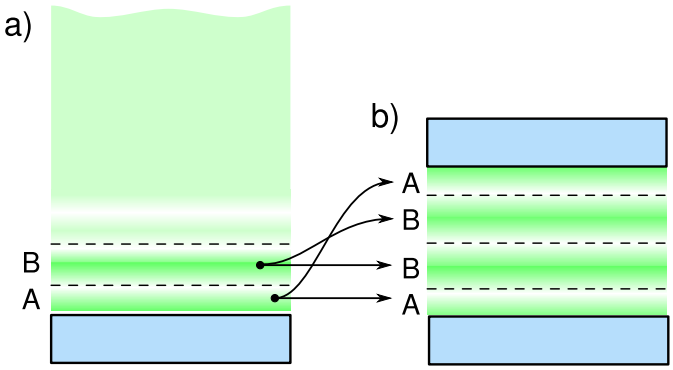

Fig. 3 (Colour online) (a) Schematic view of the film system and (b) reconstructed confined system. A refers to the first liquid layer at the interface while B labels the second layer.

was determined from equilibrium simulations of IL films. For this purpose, we created systems featuring only one silica surface and either 360 pairs of [BMIM][NTF2] or 486 pairs of [BMIM][BF4] (Fig. 3(a)). The vertical size of the simulation box was set to 16.0 nm, to ensure the presence of about 7.0 nm thick vacuum region above the fluids. The systems were first equilibrated at 600 K for 10 ns, followed by cooling down to 300 K over 5 ns, and finally by equilibrating at 300 K for 5 ns. Afterwards, both systems were simulated for 10 ns to obtain statistical quantities.

As discussed in more detail in the next section 3.1, both liquids form layered structures at the interface with silica. This allows us to estimate how many layers could fit into the confined region and thus construct the confined systems. In particular, we found that the first two molecular layers for both fluids extend roughly for 1.0 nm above the surface, thus four molecular layers are expected to be present in a 2.0 nm thick confined region. The number of molecular ion pairs to fit into the confined systems will be the one found within two IL-silica boundary layers (type A) plus two layers equivalent to the second layer of the film (type B) (see Fig. 3(b)). Thus estimated numbers of molecular ion pairs in confined fluids are 102 for [BMIM][NTF2] and 150 for [BMIM][BF4]. We also simulated the compression of the fluids between the silica slabs immersed in bulk ILs where molecular ions are allowed to move freely in and out of the confined space between slabs and obtained similar results. After these amounts of molecules are placed between the silica surfaces, the systems are relaxed again for 2 ns, before shear motion is introduced.

2.4 Simulating the shear dynamics

The shear dynamics of the confined liquids is simulated by applying a relative shear motion between the surfaces. This is done by moving the upper silica slab at constant speed v ranging between $1-200$ m/s, while keeping the lower slab fixed. Even the slowest speed $v = 1$ m/s we calculate is expected to be several orders of magnitude faster than the experimental value, and that is the lower limit reachable with available computer power.

Constant height or constant volume boundary conditions are also introduced in accord with the experimental setup, i.e. the slabs cannot freely move in the vertical direction in response to the interaction with the fluid. The load is therefore not directly applied but rather calculated as the time-average of eq.2. Nevertheless, load can be controlled through fine adjustment of the separation between the slabs. Practically,

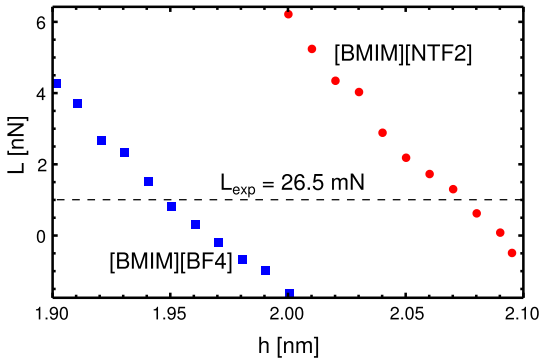

Fig. 4 (Colour online) Dependence of the average load L on the separation distance h calculated for the confined systems under shear motion at $v = 1$ m/s. The value $L_{exp} = 26.5$ mN indicated in the plot at 1 nN gives the corresponding experimental load on a macroscopic surface.

we repeated the simulation at different separation distances, within $h = 2.0 \pm 0.1$ nm, and the corresponding load is shown in Fig. 4. A small difference in separation distance of 0.01 nm can lead to a change in the load of about 0.5 nN, indicating how the liquids are incompressible.

It has to be noted that a load of 1 nN acting on our small model surface corresponds to 26.5 mN as measured on the macroscopic surface used in experiments. Thus the experimental load of about 0.3 mN would be matched in our calculation by an average load of 0.014 nN. Unfortunately, determining the separation distance that yields this small value is quite challenging because of the steep dependence of load on the distance. Moreover, as it will be shown in section 3.3, fluctuations in the forces experienced by the slabs are quite large, about $3-5$ nN, thus the accuracy of the average is not high enough to reliably obtain such a small value. For this reason, we focus on the analysis of shear dynamics under the two

Table 1 Surfaces separation and averaged load for the selected simulations.

System	h (nm)	Load (nN)
[BMIM][NTF2]	2.095	-0.42
[BMIM][NTF2]	2.040	2.91
[BMIM][BF4]	1.980	-0.64
[BMIM][BF4]	1.920	2.75

qualitatively opposite conditions of high and low load. The conditions for the chosen simulations are reported in Table 1.

3 Results

Below we discuss the results of our simulations predicting the structure of confined ILs and their behaviour under shear. We start from presenting the results of equilibrium simulations for liquid films and then analyse the shear dynamics.

3.1 Liquid Films

Besides allowing the accurate estimation of the IL amounts in the confined system, the equilibrium simulations of films give important information on the ordering of the ILs at the interface with hydroxylated silica.

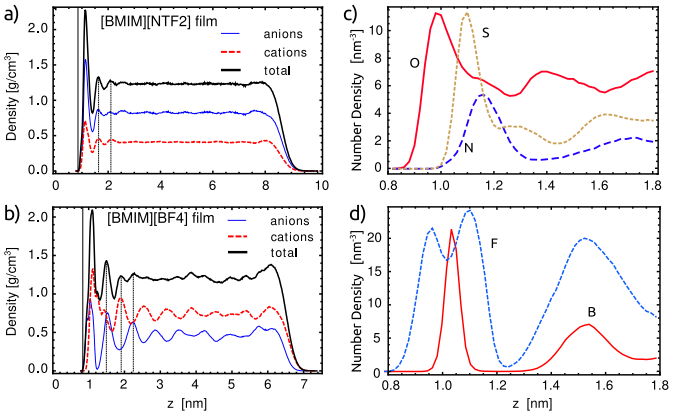

Fig. 5 (Colour online) Density profiles for (a) [BMIM][NTF2] and (b) [BMIM][BF4] films adsorbed on silica for anions (solid blue) and cations (dashed red) separately; the total densities are represented by thick black lines. The vertical black line indicates the average height of the surface OH groups at 0.836 nm. (c) Average distribution of O, S and N atoms in the first two layers of [BMIM][NTF2]. (d) Average distribution of B and F atoms in the first two layers of [BMIM][BF4]. All quantities were averaged over 10 ns simulations after the initial equilibration.

Molecular layers of [BMIM][NTF2] having thickness of about 0.5 nm are clearly seen up to 1.5 nm above the surface(see Fig. 5(a)). The separate contributions from the two molecular species show density peaks at the same heights and analysis of these peaks revealed that each layer contained roughly the same amount of anions and cations, being effectively neutral. The content of the first two anion peaks was resolved into its atomic contributions, as shown in Fig. 5(c). In the first layer, O atoms are found closest to the surface, suggesting that the majority of NTF2 molecules are adsorbed horizontally on the surface. O and S peaks for the first layer appear as a superposition of multiple structures.

In contrast, layers apparently only 0.35 nm apart, are visible over the whole height of the [BMIM][BF4] film (see Fig. 5(b)). Density profiles for the individual molecular species show how layers with a majority of cations are found between layers of anions. The distribution of F atoms (Fig. 5(d)) in the first layer shows two features, located around the B atoms, reflecting the preferential orientation of BF4 anions. The lack of such structure in the second peak indicates that the angular ordering is lost from this point.

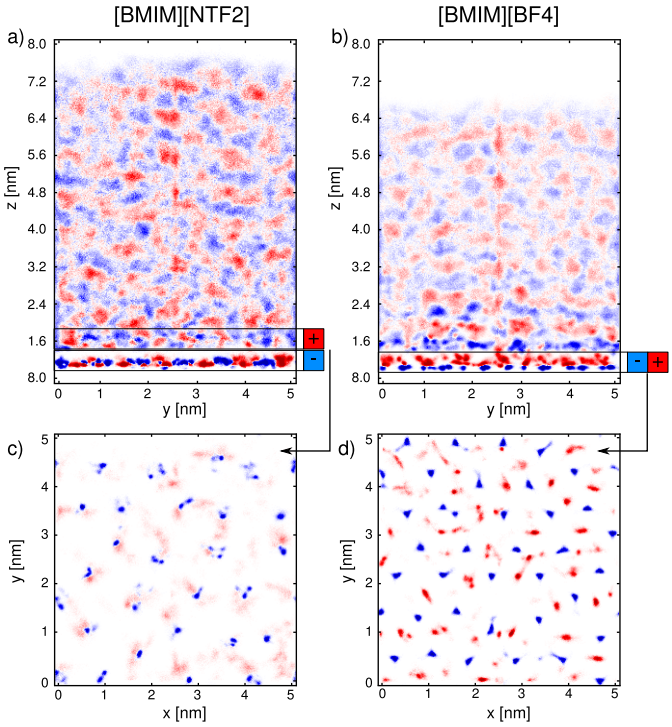

Fig. 6 (Colour online) Projected n_{diff} along the x axis for (a) [BMIM][NTF2] and (b) [BMIM][BF4] films. (c) Spatial distribution in the surface plane of the difference between n_{anion} in first layer and n_{cation} in the second layer for [BMIM][NTF2]. (d) Spatial distribution in the surface plane of the difference between n_{anion} and n_{cation} in first layer of [BMIM][BF4] film. In all plots blue and red indicate a prevalence of anions or cations respectively. The densities were averaged over 5 ns long trajectories.

To better characterise the structure of the fluids at the solid

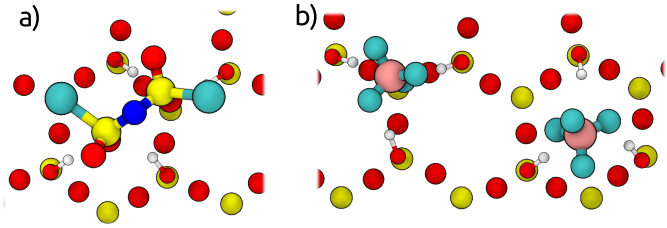

Fig. 7 (Colour online) Most probable adsorption configuration for (a) NTF2 and (b) BF4 anions on the surface.

interface, we calculated the time-averaged difference n_{diff} between the anion and cation number densities:

$$n_{diff} = \langle n_{cation} - n_{anion} \rangle_{time}$$

The number density of cations n_{cation} is calculated from the position of the imidazolium ring, while the anion densities n_{anion} are obtained from the atomic positions of N and B atoms for NTF2 and BF4 molecules, respectively.

The differential density of [BMIM][NTF2] in Fig. 6(a)) shows how the first layer is made of localised anions and cations, and how the ordering is rapidly lost. In order to understand the spatial distribution of molecules in the surface plane we calculated the difference between n_{cation} in the second layer and n_{anion} in the first layer (Fig. 6(c)). The plot reveals that cations in the second layer are located mostly above the anions of the first layer. The structure of the liquid at the interface appears to be similar to an fcc (001) surface. Anions and cations in boundary layer of [BMIM][BF4] are clearly separated in two layers (Fig. 6(b)), and this stacking remains visible far from the interface. The in-plane distribution of the first cation and anion layer in Fig. 6(d) reveals their alternating pattern. This configuration is more similar to an fcc (111) surface of binary ionic crystals. In both cases, the structure is not perfect and defects can be observed. These are caused by the mismatch between the equilibrium structure of the ILs and the surface structure, particularly positions of silanol groups.

Figure 7 shows the most frequently observed adsorption configuration for anions on the surface. NTF2 is found aligned with the surface with each sulphonyl group located between two adjacent silanol groups. BF4 anions, being much smaller, are sitting inside the triangles formed by silanol groups. Fig. 7(b) shows the two possible locations and, despite the two are not equivalent from a structural point of view, no clear preference for BF4 is observed.

3.2 Shear Dynamics

Below we provide the detailed analysis of MD trajectories for the simulations conditions reported in Table 1. We restrict the analysis to the slowest speed $v = 1$ m/s that could be simulated, which is the closest to the experimental situation.

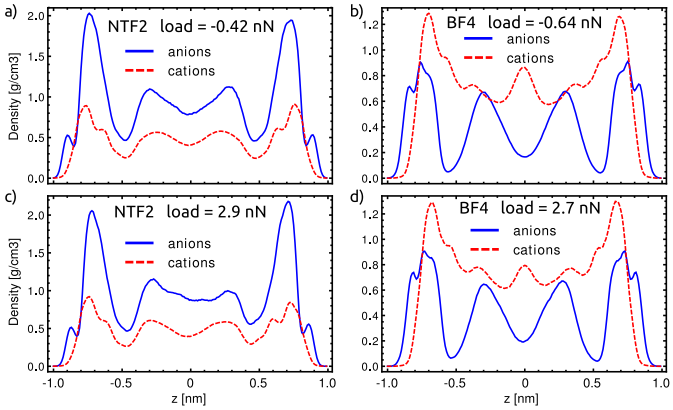

Fig. 8 (Colour online) Density profiles for the confined liquids under shear stress calculated in (a,b) low and (c,d) high load conditions. Blue lines show the density profiles of anions, dashed red lines represent the density of cations. The profiles were averaged over 10 ns of simulation at shear velocity of 1 m/s.

Fig. 8 shows the density profiles of the confined fluids during shear motion. [BMIM][NTF2] layers (Fig. 8(a,c)) are mostly neutral and the density peaks for anions and cations appear at the same positions as seen in the films. The density in the inner layers appears as asymmetric peaks at low load, and this feature is more pronounced at high load where multiple overlapping peaks appear.

[BMIM][BF4] (Fig. 8(b,d)) exhibits alternating layers with one prevalent molecular species, and both anion and cation density profiles consist of sharply defined peaks. The boundary anion layers consist of multiple features, suggesting that molecules have a preferential orientation. No major differences depending on the load are found.

We divide the confined volume in four layers, as suggested by the density profiles of anions, and calculate the velocity of each molecular layer. This analysis gives us information about the type of flow, and helps to distinguish fluid from solid-like regimes.

The lower and upper boundary layers are defined as corresponding to $z < -0.5$ nm and $z > 0.5$ nm, respectively. The lower middle layer lies in the region $z \in [-0.5, 0]$nm and the upper middle layer us defined by $z \in [0, 0.5]$nm. Fig. 9 shows the time evolution of the anion velocity in each layer of the fluids, where each point is averaged over 500 ps to clear the noise. In all cases, boundary layers drift with speed similar to their adjacent surfaces although the fluctuations are different for the two systems. Large amplitude fluctuations with slow timescale are observed in [BMIM][NTF2]; at high load the timescale appear even slower (Fig. 9(a,c)). In [BMIM][BF4], on the other hand, smaller and faster variations are observed, and the velocities of the middle layers are much more similar to the velocities of their adjacent boundary layers regardless

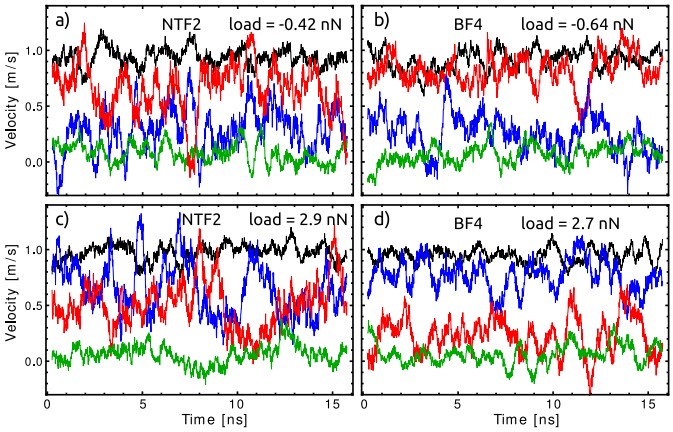

Fig. 9 (Colour online) Time-dependent average velocity of the anions in each layer of (a,c) [BMIM][NTF2] and (b,d) [BMIM][BF4] at low and high load. Green lines represent the boundary layer on the lower surface, red and blue lines give the lower and upper middle layers respectively, and black line shows the boundary layer on the upper surface.

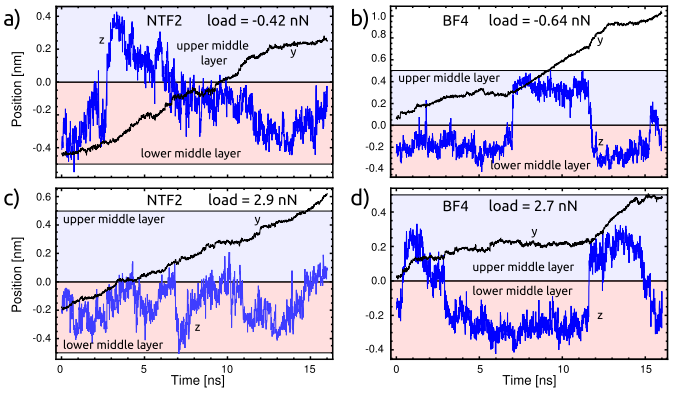

Fig. 10 (Colour online) Trajectory of a molecule in the inner layers of [BMIM][NTF2] at (a) low and (c) high load. The trajectory of a [BMIM][BF4] molecule under low and high load are reported in (b) and (d) respectively. The vertical position is marked by the blue lines, while the lateral position in the shear direction is scaled down by a factor of 10 and represented by the black lines. The red area marks the region considered as lower middle layers where $z \in [-0.5, 0]$nm, and the blue area at $z \in [0, 0.5]$nm marks the upper middle layer, closer to the moving surface.

of the load (Fig. 9(b,d)).

Fig. 10 shows 16 ns portions of the trajectories of anions located within the middle layers for both fluids. The black line, showing the lateral drift of the molecule, is scaled down by a factor of 10 in order to fit in the same scale as the vertical position. The central N atom in NTF2 is used to track the molecular position, while the B atom is used for BF4. The trends observed for these particular molecules are common to all the molecules found in the same layers and are thus representative for the systems. In both cases the last 16 ns of longer trajectories are plotted. Vertical motion of NTF2 molecules (Fig. 10(a,c)) features both slow fluctuations and sudden jumps between the two inner layers. The lateral drift appears uniform with small occasional jumps.

The motion of BF4 molecules (Fig. 10(b,d)) is quite different as they tend to fluctuate quickly within one layer until suddenly jumping to the adjacent one. While the molecule is in the lower layer no drift is visible and it occasionally advances in the shear direction by small sudden jumps. In the upper layer, the lateral velocity is higher and the motion appears more uniform. The behaviour of both fluids does not seem to be affected by the load. The statistical analysis of whole trajectories, reported in Table 2, reveals that NTF2 anions exhibit twice as many interlayer jumps than BF4.

3.3 Lateral Forces and Load

The dynamics of fluids impacts the overall forces acting on the silica surfaces. Fig. 11 shows the trend of lateral $F_{lat}(t)$, and normal $L(t)$ forces acting on the slabs for the two systems. When the raw data are averaged over 20 consecutive samples,

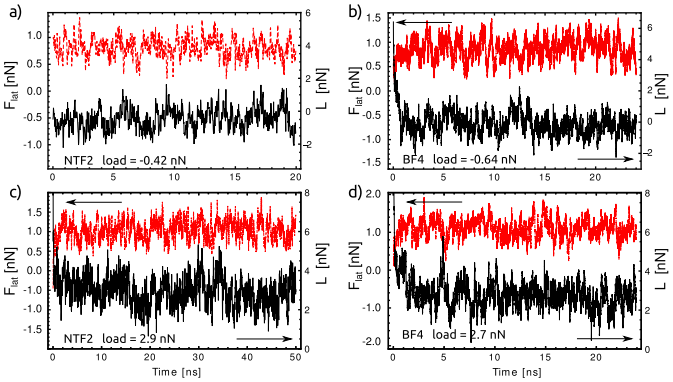

Fig. 11 (Colour online) Total forces acting on the sliding surface for (a) [BMIM][NTF2] and (b) [BMIM][BF4] at small load and (c,d) at large load. Red dashed lines show the lateral force (scale on the left axis) and the solid black lines represent the normal load (scale on the right axis). Each point represents the average value over 20 ps.

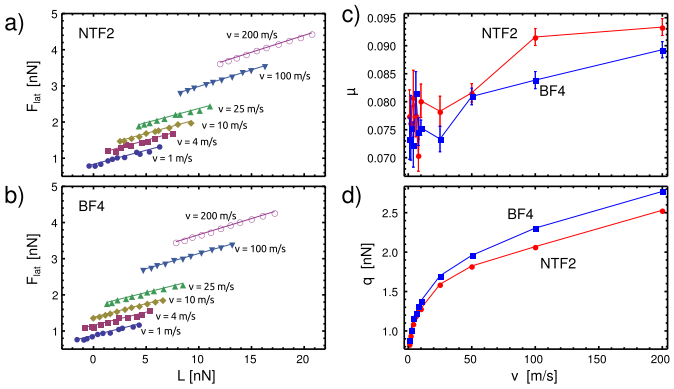

Fig. 12 (Colour online) Average lateral and normal forces obtained from the shear calculations for (a) [BMIM][NTF2] and (b) [BMIM][BF4]: different symbols represent the values calculated varying the separation distance with the same shear velocity. The lines represent the result of linear fits for each constant velocity dataset. (c) Friction coefficient obtained from the linear fit of the data in (a) and (b): the error bars are given by the standard error of the linear regression. (d) Offset value of the linear fit: the standard errors are just smaller than the size of the dots, thus not visible.

the fluctuating trend of $F_{lat}(t)$ becomes visible and exhibits features quite similar to chaotic stick-slip friction.

Fluctuations in the normal load $L(t)$ of about 3 nN amplitude are observed in both systems and at either load. [BMIM][NTF2] shows a weak dependence on load, as the magnitude of the fluctuations appears increased to 5 nN and slow timescale components become visible over tens of nanoseconds at high load (see Fig. 11(c)). In [BMIM][BF4] fluctuations appear with shorter time scale and smaller amplitude (Fig. 11(b,d)), while the load again has no clear effect.

Table 2 Statistical analysis of molecular behaviour and fluctuations in forces.

	Load (nN)	Jumps (GHz)	$\sigma(F_{lat})$	$\sigma(L)$
[BMIM][NTF2]	-0.42	0.48	0.54	1.02
[BMIM][NTF2]	2.91	0.52	0.56	1.06
[BMIM][BF4]	-0.64	0.22	0.50	0.98
[BMIM][BF4]	2.75	0.23	0.51	0.99

This behaviour can be quantified by the standard deviation of $F_{lat}(t)$ and $L(t)$ with the results reported in Table 2. Standard deviations for [BMIM][NTF2] are by about 7% larger then [BMIM][BF4] and show a weak dependence on the load.

In order to evaluate the friction coefficient for our ILs, we performed simulations at different separation distances and shear velocities. The resulting average $F_{lat}(t)$ are plotted against the average $L(t)$ in Fig. 12(a-b). Each data point was calculated from the average of a 10 ns long simulations, after additional 2 ns of equilibration. The data points obtained at the same constant speed appear well aligned. Therefore we fitted all the sets using a modified Amonton's law:

$$F_{lat} = \mu L + q, \tag{3}$$

where μ is the friction coefficient and q the offset related to adhesive interactions at the liquid-surface interface. The values of μ are plotted in Fig. 12(c) against the shear velocity. The value for [BMIM][NTF2] appears slightly larger than [BMIM][BF4] and there seems to be a small increase in the friction coefficient with sliding speed. At slow speed the estimation is quite noisy due to the worse averaging. The adhesive contribution (Fig. 12(d)) increases with shear velocity, and it is always larger for [BMIM][BF4].

4 Discussion

We will now discuss our findings and how they compare to previous experimental work as well as some of the limitations of our model.

We start from the bulk viscosity of ILs. In our preliminary studies on the bulk liquid systems (not shown here), we were able to calculate the bulk viscosity of the ILs using the Einstein's relations, although extremely long simulations were necessary. The calculated values of 55 mPas (exp. 40 mPas) for [BMIM][NTF2] and 91 mPas (exp. 75 mPas) for [BMIM][BF4], despite being larger than experimental ones, show that [BMIM][BF4] has higher viscosity than [BMIM][NTF2], which can be qualitatively explained by simple geometric arguments.

The molecular structure of bulk ILs is determined by the stronger electrostatic interaction in standard conditions. Their structure is then similar to the fcc structure of binary ionic crystals but, since the ions are not point charges, the shape of the molecules will affect the stability of the overall structure and therefore viscosity. The negative charge in NTF2 anions is located mostly on the O atoms of the sulphonyl groups, at the extremities of the molecules. Therefore, the structure of the bulk liquid will allow more configurations of similar energy and the system can easily shear between them. The charge on BF4 is more localized on a much smaller and spherical molecule, thus the overall structure will be more stable and resilient to shear motion. This trend is observed in many ILs, as reported in Table 1 of Ref.[31], and it seems to be a general property of ILs.

Similar consideration can be applied to the confined systems and, even though the situation is quite different, the model proposed here still explains the results.

The structure of the films for the two ILs are very distinct from each other (Fig. 5 and 6). [BMIM][NTF2] forms neutral layers containing the same amount of cations and anions, but [BMIM][BF4] arranges in alternating charged layers where one molecular species was more abundant than the

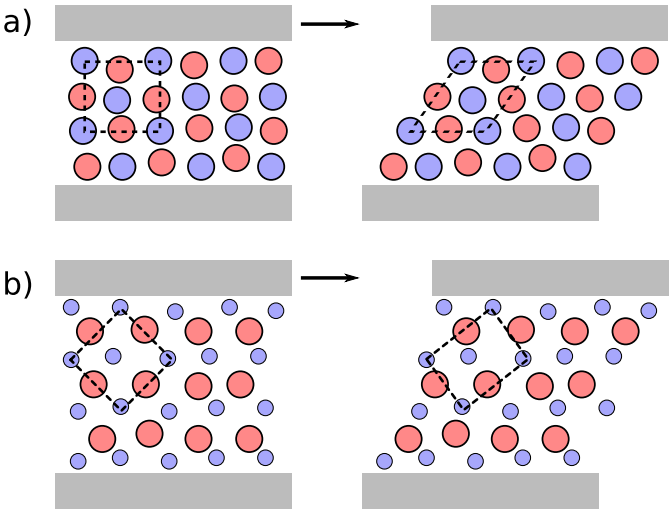

Fig. 13 (Colour online) Schematic representation of the shear dynamics for a fluid ordered in (a) neutral layers as [BMIM][NTF2] and (b) alternating charged layers like [BMIM][BF4]. Blue and red sphere represent the anions and cations respectively. The dashed square marks the unit cell of the liquid.

other. These features are also seen in the confined systems under shear stress (Fig. 8).

This effect can be attributed to the smaller size of BF4 anions, allowing them to be closer to the surface. BMIM cations, being larger, cannot approach as close and stay slightly above the first BF4 layer. At this point, other BF4 anions, feeling the repulsion from the adsorbed BF4, cannot occupy the same layer as the first BMIM layer and are stacked on top of it. The liquid interface appears similar to the fcc (111) surface of ionic crystals, stabilised by the interaction with silica. NTF2 anions are larger and elongated, and, even though their O atoms are found close to the surface, the other atoms (N and CF_3 groups) are further away. BMIM cations can then arrange themselves into the same range of heights, filling the space between anions. The interface has a structure closer to the fcc (001).

The alternating layer structure in ILs, like the one seen in [BMIM][BF4], has been observed before in different systems [16,17]. It is usually attributed to the surface charge of mica inducing the separation between ions at the interface. In our case, the hydroxylated silica surface is neutral and the alternate layering is a purely geometric effect governed by the size of the molecules and their commensurability with the surface structure.

The shear dynamics of the two nanoconfined fluids is strongly dependent on the stability of their structures under shear stress. Fig. 13 illustrates the equilibrium arrangement of the two nanoconfined fluids and the perturbation introduced when shearing the top surface. In both cases boundary layers are attached to their respective surface. As the top layer shears, the structure of [BMIM][NTF2] (Fig.13(a)) becomes progressively more unstable since ions of the same type in adjacent layers start facing each other. Eventually, the instability will become more dramatic and trigger an overall rearrangement of the inner molecular layers, reaching a more stable configuration. We can see the effect of reconstruction in the density profiles of [BMIM][NTF2] in Fig. 8(a,c), where the density of the two middle layers appears as asymmetric peaks. The averaged profile is actually revealing the anions slowly fluctuating between the two layers. The detailed molecular trajectories in Fig. 10(a,c) reveal the slow and irregular fluctuations of the molecules, and the average layer velocities in Fig. 9(a,c) indicate the presence of a chaotic flow in the fluid. This chaotic dynamics results from the inability of the IL to recover the instability induced by shear and is enhanced at higher load due to the loss of mobility under tighter confinement. If the liquid is structured in alternating charged layers, ions of the same charge will not approach as close because there will always be a layer of opposite charge in between (Fig. 13(b)). The instability appears intuitively less dramatic and easier to overcome. [BMIM][BF4] is much closer to this model, although anion layers contain a small portion of cations (Fig. 8(b,d)). The well-defined peaks in confined [BMIM][BF4] density profiles indicate how the fluid keeps its layer structure under shear motion. The small vertical fluctuations of the anions observed in Fig. 10(b,d) are the signature of the fluid response to the instability. Inter-layer jumps happen quickly and occur at a much lower rate than for [BMIM][NTF2]. Anion layers can be clearly distinguished by their average velocities (Fig. 9(b,d)), well correlated to their height, in what appears as laminar flow.

These differences in the molecular flow appear also in the average forces acting on the surfaces. For both fluids lateral and normal forces fluctuate over time and show a behaviour similar to chaotic stick-slip (Fig. 11). Fluctuations for [BMIM][NTF2] are larger and slower, since the fluid does not respond quickly to the instability induced by shear. Smaller fluctuations in the forces are observed for [BMIM][BF4], indicating a slightly faster dynamics, although the signals are quite noisy and variations can still be seen on long time scales. This is the result of the slow dynamics expected in all ILs, although our simulations were able to point out the fine difference between the two considered liquids.

As a consequence of the slow dynamics, the friction coefficient cannot be accurately extracted from fitting the data points in Fig. 12(a-b), especially at slow shear velocity where the averaging is worse. Even though the calculated values qualitatively agree with experimental reports (0.08-0.1) over all the simulated shear velocities and it appears that [BMIM][NTF2] gives higher friction than [BMIM][BF4], we cannot discuss the velocity dependence of the friction coefficient in detail. The adhesive contribution to friction (Fig. 11(d)) shows a monotonic increase with shear speed for

both fluids. It is slightly larger for [BMIM][BF4]: this reflects the fact that BF4 anions in the boundary layers are better trapped by silanol groups than NTF2, which can rotate, unpinning one of the sulphonyl groups, and drifts faster.

Nevertheless, the lateral force showed a linear dependence on load in all our simulations, indicating that the fluids are always in the same frictional regime. As previously stated, the load in our simulation is much larger than that of typical experiments, both in the repulsive regime (positive load) and in the attractive one (negative load). Despite the apparent wide range of loads we tested, no changes in the friction coefficient are seen. This result is consistent with previous experiments in Ref. [16], where the friction coefficient of the IL was constant under different applied load, as long as the number of layers is preserved, up the instrumental limit of about 0.35 mN.

5 Conclusions

In conclusion, we have demonstrated how the shape of IL molecules affects their layering structure above hydroxylated silica. Our simulations showed how the structure of the liquids in nanoconfined spaces determines their dynamical properties at molecular level. When [BMIM][NTF2] is sheared, larger molecular fluctuations in the inner layers are required to stabilise the system and the resulting dynamics is irregular. The alternating charged layers in [BMIM][BF4] allow the system to stabilise through smaller oscillations, and the layers appear to shear on top of each other in a laminar fashion. The simulated dynamics explains qualitatively the change in relative viscosity that the two ILs exhibit when confined, as it was observed in previous experiments [14], even though quantitative comparison with experiments is still not possible for a variety of reasons.

Although we observed how the ordering of the fluid on the surface depends on the shape of IL molecules, the atomic structure of the surface is an important factor as well. Future studies should be focused on understanding the balance of the two contributions. It is important to address this question since it is generally accepted that the anti-wear properties of IL based lubricants come from the formation of an electric double layer that prevents asperities from getting too close to each other. In this sense, it would be desirable to design a lubricant where such anti-wear mechanism is mostly intrinsic and not dependent on particular properties of the surface.

Acknowledgements

This work was supported by World Premier International Research Center Initiative (WPI), MEXT, Japan, and by the Core Research for Evolutional Science and Technology (CREST) program of the Japan Science and Technology Agency (JST). The authors wish to thank Dr. Peter Spijker and Prof. Kazuto Akagi for helpful discussion.

References

1 J. S. Wilkes and M. J. Zaworotko, *J. Chem. Soc., Chem. Commun.*, 1992, **0**, 965–967.
2 S. A. Forsyth, J. M. Pringle and D. R. MacFarlane, *Aust. J. Chem.*, 2004, **57**, 113–119.
3 N. V. Plechkova and K. R. Seddon, *Chem. Soc. Rev.*, 2008, **37**, 123–150.
4 D. Chen, G. Wang and J. Li, *The Journal of Physical Chemistry C*, 2007, **111**, 2351–2367.
5 G. Feng and P. T. Cummings, *The Journal of Physical Chemistry Letters*, 2011, **2**, 2859–2864.
6 G. M. Whitesides, *Nature*, 2006, **442**, 368.
7 A. E. Somers, P. C. Howlett, D. R. MacFarlane and M. Forsyth, *Lubricants*, 2013, **1**, 3–21.
8 C. Ye, W. Liu, Y. Chen and L. Yu, *Chem. Commun.*, 2001, **0**, 2244–2245.
9 W. Liu, C. Ye, Q. Gong, H. Wang and P. Wang, *Tribology Letters*, 2002, **13**, 81–85.
10 Q. Lu, H. Wang, C. Ye, W. Liu and Q. Xue, *Tribology International*, 2004, **37**, 547 – 552.
11 B. Phillips and J. Zabinski, *Tribology Letters*, 2004, **17**, 533–541.
12 R. González, A. Hernández Battez, D. Blanco, J. Viesca and A. Fernández-González, *Tribology Letters*, 2010, **40**, 269–277.
13 B. Yu, D. G. Bansal, J. Qu, X. Sun, H. Luo, S. Dai, P. J. Blau, B. G. Bunting, G. Mordukhovich and D. J. Smolenski, *Wear*, 2012, **289**, 58 – 64.
14 K. Ueno, M. Kasuya, M. Watanabe, M. Mizukami and K. Kurihara, *Physical Chemistry Chemical Physics*, 2010, **12**, 4066.
15 I. Bou-Malham and L. Bureau, *Soft Matter*, 2010, **6**, 4062–4065.
16 A. M. Smith, K. R. J. Lovelock, N. N. Gosvami, T. Welton and S. Perkin, *Phys. Chem. Chem. Phys.*, 2013, **15**, 15317–15320.
17 M. Mezger, H. Schröder, H. Reichert, S. Schramm, J. S. Okasinski, S. Schöder, V. Honkimäki, M. Deutsch, B. M. Ocko, J. Ralston, M. Rohwerder, M. Stratmann and H. Dosch, *Science*, 2008, **322**, 424–428.
18 G. Feng, J. S. Zhang and R. Qiao, *The Journal of Physical Chemistry C*, 2009, **113**, 4549–4559.
19 M. Sha, G. Wu, Q. Dou, Z. Tang and H. Fang, *Langmuir*, 2010, **26**, 12667–12672.
20 R. Hayes, N. Borisenko, M. K. Tam, P. C. Howlett, F. Endres and R. Atkin, *The Journal of Physical Chemistry C*, 2011, **115**, 6855–6863.
21 R. Hayes, S. Z. El Abedin and R. Atkin, *The Journal of Physical Chemistry B*, 2009, **113**, 7049–7052.
22 J. Sweeney, F. Hausen, R. Hayes, G. B. Webber, F. Endres, M. W. Rutland, R. Bennewitz and R. Atkin, *Phys. Rev. Lett.*, 2012, **109**, 155502.
23 Y. Mo, K. T. Turner and I. Szlufarska, *Nature*, 2009, **457**, 1116.
24 M. Urbakh and E. Meyer, *Nat Mater*, 2010, **9**, 8–10.
25 F. Dommert, K. Wendler, R. Berger, L. Delle Site and C. Holm, *ChemPhysChem*, 2012, **13**, 1625–1637.
26 H. Matsubara, F. Pichierri and K. Kurihara, *Phys. Rev. Lett.*, 2012, **109**, 197801.
27 O. A. Mazyar, G. K. Jennings and C. McCabe, *Langmuir*, 2009, **25**, 5103–5110.
28 A. C. F. Mendonça, P. Malfreyt and A. A. H. Pádua, *Journal of Chemical Theory and Computation*, 2012, **8**, 3348–3355.
29 A. C. F. Mendonça, A. A. H. Pádua and P. Malfreyt, *Journal of Chemical Theory and Computation*, 2013, **9**, 1600–1610.
30 A. C. F. Mendonça, Y. D. Fomin, P. Malfreyt and A. A. H. Padua, *Soft Matter*, 2013, **9**, 10606–10616.

31 H. Tokuda, S. Tsuzuki, M. A. B. H. Susan, K. Hayamizu and M. Watanabe, *The Journal of Physical Chemistry B*, 2006, **110**, 19593–19600.

32 F. Zhou, Y. Liang and W. Liu, *Chem. Soc. Rev.*, 2009, **38**, 2590–2599.

33 X. Zhong, Z. Liu and D. Cao, *The Journal of Physical Chemistry B*, 2011, **115**, 10027–10040.

34 J. Puibasset and R. J.-M. Pellenq, *The Journal of Chemical Physics*, 2003, **119**, 9226–9232.

35 D. Argyris, N. R. Tummala, A. Striolo and D. R. Cole, *The Journal of Physical Chemistry C*, 2008, **112**, 13587–13599.

36 L. Zhuravlev, *Colloids and Surfaces A: Physicochemical and Engineering Aspects*, 2000, **173**, 1 – 38.

37 R. T. Cygan, J.-J. Liang and A. G. Kalinichev, *The Journal of Physical Chemistry B*, 2004, **108**, 1255–1266.

38 M. P. Allen and D. J. Tildesley, *Computer Simulation of Liquids*, Oxford: Clarendon, 2002.

39 R. W. Hockney and J. W. Eastwood, *Computer simulation using particles*, Taylor & Francis, Inc., Bristol, PA, USA, 1988.

40 S. Nosé, *Journal of Chemical Physics*, 1984, **81**, 511–519.

41 W. G. Hoover, *Physical Review A*, 1985, **31**, 1695–1697.

42 S. Plimpton, *Journal of Computational Physics*, 1995, **117**, 1 – 19.